Journal of Applied Polymer Science

Fabrication of ordered microporous styrene-acrylonitrile copolymer blend imprinted membranes for selective adsorption of phenol from salicylic acid using breath figure method

Fengquan Sun,[1] Minjia Meng,[1] Li Yan,[2] Zhihui He,[1] Yongsheng Yan,[1] Yan Liu,[2] Shijuan Liu[3]

[1]School of Chemistry and Chemical Engineering, Jiangsu University, Zhenjiang 212013, China
[2]School of Chemistry, Jilin Normal University, 1301 Haifeng Street, Siping 136000, China
[3]Yangzhong Jinxiang Latex Co., Great Bridge Road 88, Yangzhong, 212200, China
Correspondence to: Y. Yan (E-mail: mmjybyq@aliyun.com)

ABSTRACT: Highly selective, ordered microporous molecularly imprinted membranes (MIMs) for phenol were synthesized by breath figure (BF) method using styrene-acrylonitrile copolymer (SAN) as the membrane matrix and molecularly imprinted polymer nanoparticles (nano-MIPs) as the imprinted nanoparticles. The nano-MIPs were synthesized by oil-in-water emulsion polymerization using 4-vinyl pyridine (4-VP), methyl methacrylate (MMA) or cinnamic acid (CA) as the functional monomer, respectively. The prepared nano-MIPs were characterized by transmission electron microscope (TEM) and Raman, whereas MIMs were characterized by SEM, membrane flux, and selective adsorption experiments. Morphological analysis exhibited that the addition of nano-MIPs improved the formation of ordered and well-defined porous membrane morphology. Compared with MMA-MIM and CA-MIM, the 4-VP-MIM exhibited higher membrane flux, adsorption capacity, and stronger selective binding for phenol as well as excellent permeation selectivity for phenol. Moreover, the selective effect of 4-VP-MIM on phenol was strongly affected by the amount of 4-VP imprinted nanoparticles (nano-4-VP-MIPs). The experimental data revealed that the 4-VP-MIM containing 2.0 wt % of nano-4-VP-MIPs exhibited the highest separation selectivity for the template phenol, whose selectivity coefficients for phenol relative to salicylic acid (SA) and *p*-hydroxybenzoic acid (*p*-HB) were 5.6770 and 5.5433, respectively, which was close to the predicted selectivity coefficient value.
 J. Appl. Polym. Sci. **2015**, *132*, 42350.

KEYWORDS: adsorption; membranes; molecular recognition; separation techniques

Received 20 January 2015; accepted 8 April 2015
DOI: 10.1002/app.42350

INTRODUCTION

Salicylic acid (SA) is widely used as a prominent pharmaceutical intermediate to produce ethoxybenzamide, diuretin, glybenzcyclamide, niclosamide, bismuth subsalicylate, and sulfasalazine.[1] It is also an important material of acetylsalicylic acid (ASA), usually called aspirin, which has been reported as the world's first truly synthetic drug possessing anti-inflammatory activity against rheumatism.[2,3] However, on account of the incomplete conversion of raw materials and poor general separation technology in the industrial SA production, phenol as a concomitant of SA is often detected in SA product. The excess concentration of phenol will enhance the harmful effect to human health and cause negative effect on the brain, digestive system, heart, kidney, liver, peripheral nerve, and the unborn child due to its chemical stability, water solubility, and environmental mobility.[4] Additionally, the traditional separation technology seems impossible to effectively recycle of phenol in the aqueous solution and turn "waste" into wealth. Therefore, it is of necessity to find efficient technique for the selective separation of phenol from SA for ensuring the purity of SA product.

Molecularly imprinting technology (MIT), which was firstly introduced by Wulff and Sarhan[5] in 1972, has become a powerful method in the field of separation and purification. Up to date, MIT has made some advances in selectively separation of various compounds[6] in selective recognition studies.[7,8] Recently, the molecularly imprinted membrane (MIM) has become one of the research focuses in the separation field by combining the MIT with membrane technology.[9] Wu *et al.*[10] successfully used surface imprinted poly(vinylidene fluoride) (PVDF) membrane for selective separation of artemisinin (Ars) from artemether, which showed high selectivity and chemical stability. Donato *et al.*[11] prepared a novel hybrid MIMs by the water phase

Additional Supporting Information may be found in the online version of this article.

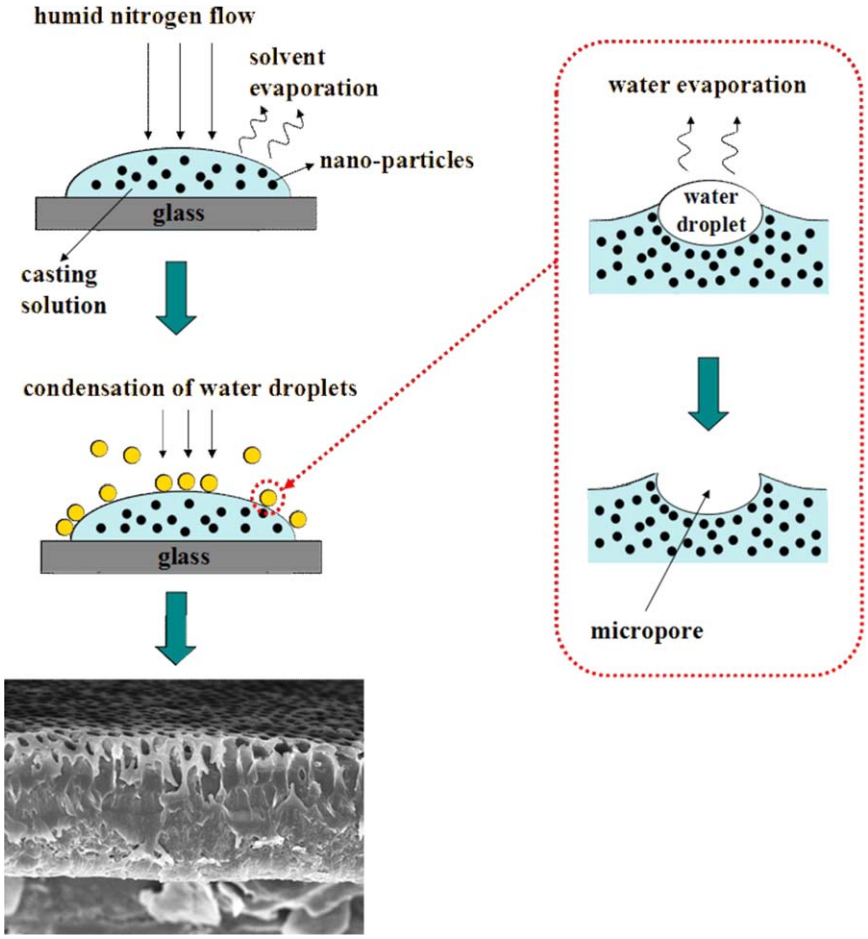

Figure 1. Schematic illustration of preparing SAN blend imprinted membranes by BF method. [Color figure can be viewed in the online issue, which is available at wileyonlinelibrary.com.]

precipitation polymerization method with the ability to specially recognize 4,4′-methylendianiline from its structural analogue 4,4′-ethylendianilinein in isopropanol. Compared to conventional separation techniques, MIM is capable to separate target molecules from solutions by simple permeation through the membranes. However, the known limits of such MIM are the following: easy to be blocked, low mass-transfer rate or complex synthetic method.[12] Therefore, it is urgent to develop a new method to fabricate imprinted membranes with high separation performance.

Recently, the ordered microporous membranes is a center of interest currently, which possess extremely high surface areas of membranes, thus allowing their employment in a large variety of applications.[13,14] The well-established breath figure (BF) method seems to be a promising, low-cost, and self-assembly method to fabricate ordered microporous membranes, which was first discovered by François and coworkers.[15,16] Liu *et al.*[17] successfully fabricated ordered honeycomb porous polyvinyl chloride (PVC) membranes via BF method. Han *et al.*[18] investigated the effect of combining BF method with replica molding methods for fabrication of polypyrrole membrane with microlens arrays. Results show that the membrane morphology is strongly improved by using BF method. However, there are few reports[19] on fabrication of MIM by combining the MIT and BF method. The main challenge in combining MIT and BF technique: one for selectively recognizing templates and another one for forming the ordered microporous membrane morphology. Thus, the BF imprinting (Figure 1) was followed in the present study: the molecularly imprinted polymers nanoparticles (nano-MIPs) was firstly prepared via an oil-in-water emulsion polymerization process containing templates.[20] Then, the mixture solution was obtained by dissolving matrix and nano-MIPs in a highly volatile and poorly water soluble solvent. Casting the mixture solution on a substrate under a flow of moistened nitrogen at a relative high humidity, the microporous membrane with binding sites, and specific membrane morphology was formed when the solvent completely evaporated.[21,22] Therefore, the aim of the present study is to develop the MIM with ordered porous morphology and to investigate the performance of the template recognition and molecule transfer process.

In this work, the imprinted nanoparticles for phenol were firstly prepared by imprinting technique oil-in-water emulsion polymerization in the presence of 4-vinyl pyridine (4-VP), cinnamic acid (CA), and methyl methacrylate (MMA) as the functional monomer, respectively. The MIMs with ordered microporous morphology and recognition sites for phenol were synthesized

Table I. The nano-MIPs Obtained by an Oil-in-water Emulsion Polymerization Process with Different Functional Monomer Amounts

Imprinted and non-imprinted nanoparticles	Compositions of pre-polymerization solution			
	phenol (mmol)	4-VP (mmol)	MAA (mmol)	CA (mmol)
nano-4-VP-MIPs	0.1	0.6	0	0
nano-4-VP-NIPs	0	0.6	0	0
nano-MMA-MIPs	0.1	0	0.4	0
nano-MMA-NIPs	0	0	0.4	0
nano-CA-MIPs	0.1	0	0	0.2
nano-CA-NIPs	0	0	0	0.2

by using BF method with styrene-acrylonitrile copolymer (SAN) as matrix, chloroform as solvent, and imprinted nanoparticles as functional polymers. The influences of imprinted nanoparticles on membrane morphology and the selective separation performance towards phenol of the MIMs were evaluated and investigated.

EXPERIMENTAL

Materials

Phenol, styrene (St), chloroform, dodecyltrimethylammonium bromide (DTAB), and potassium persulfate (KPS) were all supplied by Sinopharm Chemical Reagent (Shanghai, China). SA, *p*-hydroxybenzoic acid (*p*-HB), CA, 4-VP, MMA, and divinylbenzene (DVB) were obtained from Aladdin reagent. Monomers were washed by sodium hydroxide aqueous solution to remove inhibitors and stored in dry conditions prior to use. SAN was purchased from Shanghai JieSu Import and Export Co. All other chemicals used were of analytical grade and obtained commercially. Doubly distilled water used throughout the experiments was obtained from laboratory purification system.

Ultraviolet Visible (UV) Spectrophotometry Study

In order to evaluate the optimal molar ratios of the template (phenol) to functional monomer (4-VP, MMA, and CA), the ultraviolet visible (UV) spectrophotometry was used for analysis. The polymeric dope solutions (10 mL) were prepared in the colorimetric tubes, which contained template phenol (0.1 mmol) and functional monomer (4-VP, MMA or CA) with different concentrations ranging from 0 mmol to 1.2 mmol. The absorbance of phenol at 218 nm in the mixture solutions were observed by UV spectrophotometry.

Synthesis of Molecularly Imprinted Nanoparticles (nano-MIPs) and Non-Imprinted Nanoparticles (nano-NIPs)

The nano-MIPs were prepared via an oil-in-water emulsion polymerization process containing templates.[23] Firstly, DTAB (1.0 g), phenol (0.1 mmol), and distilled water (20 mL) were added into a 50 mL flask, stirring at room temperature for 1.0 h in order to form the aqueous solution. Secondly, St (2.0 mL) and DVB (0.8 mL) were mixed with methanol solution (2.3 mL) containing 0.6 mmol (or varied amounts) of functional monomer (4-VP, MMA or CA), as summarized in Table I. The mixture was added dropwise into the aqueous solution within 2.0 h in order to obtain micelles in the oil-in-water solution. Thereafter, 0.04 g of initiator (KPS) was added into the oil-in-water solution with nitrogen for 10 min to eliminate oxygen. The solution was sealed for polymerization at 70°C for 3.0 h. Finally, the nano-MIPs were obtained after washing by excessive methanol and drying.

The non-imprinted nanoparticles (nano-NIPs) were prepared in the same process without the template. In comparison, the nano-MIPs and nano-NIPs were prepared analogously except the presence of template phenol in the above aqueous solution.

Synthesis of SAN Blend Imprinted and Non-Imprinted Membranes

The SAN blend membranes were prepared according to composition given in Table II. At first, the 10 mg mL^{-1} nano-MIPs nanofluids were obtained by dispersing 0.02 g nano-MIPs into 2.0 mL ethanol completely using tip ultrasound equipment for 10 min. Then, the homogeneous casting solution was prepared by uniformly adding the SAN into the chloroform containing amount of nano-MIPs nanofluid. Thereafter, the blend imprinted membranes were obtained by using the BF method. Specifically, the casting solutions were transferred quickly onto a clean glass substrate using a micro-syringe under a humid flow at a controlled relative humidity (RH) of 75%. The RH was controlled by the flow of a proper quantity of moist nitrogen through the pipe. After complete evaporation, the microporous imprinted membrane with binding sites for phenol was formed on such glass slide and obtained after drying at 25°C.

Finally, the SAN blend imprinted membranes were extracted with mixed solvents of methanol/acetic acid (9 : 1, v/v) in a Soxhlet apparatus to remove the template. The SAN non-imprinted membranes were fabricated in the presence of the nano-NIPs using the same method. The blank SAN membrane was also prepared in the absence of nanoparticles and subjected to the same procedure.

Characterization

The nano-MIPs were characterized by transmission electron microscope (TEM, JEM-2100) and Raman spectra (DXR) with a WITEC Spectra Pro 2300I spectrometer which equipped with an Ar-ion laser and provided a laser beam of 532 nm wavelength. The surface morphologies and cross-sectional structures of the prepared membranes were obtained by scanning electron microscope (SEM, S-4800).

Table II. Membrane Composition for all Prepared SAN Blend Membranes

	Compositions of casting solution (wt %)				
Membrane	SAN	chloroform	nano-MMA-MIPs nanofluid	nano-CA-MIPs nanofluid	nano-4-VP-MIPs nanofluid
Blank SAN membrane	3.0	97	0	0	0
MMA-MIM	3.0	95.5	1.5	0	0
CA-MIM	3.0	95.5	0	1.5	0
4-VP-MIM0	3.0	96	0	0	1.0
4-VP-MIM1	3.0	95.5	0	0	1.5
4-VP-MIM2	3.0	95	0	0	2.0
4-VP-MIM3	3.0	94.5	0	0	2.5
	Compositions of casting solution (wt %)				
Membrane	SAN	chloroform	nano-MMA-NIPs nanofluid	nano-CA-NIPs nanofluid	nano-4-VP-NIPs nanofluid
MMA-NIM	3.0	95.5	1.5	0	0
CA-NIM	3.0	95.5	0	1.5	0
4-VP-NIM1	3.0	95.5	0	0	1.5

Membrane Flux Experiments

The membrane was fitted on the ultrafiltration cell (UF-8010, Amicon) with the effective membrane area 4.9 cm^2, and the aqueous solution containing 100 mg L^{-1} phenol was prepared as the feed solution to measure the membrane flux. The feed solution permeated through different membranes under the steady operation pressure 0.15 MPa. The flux of the different membranes could be calculated by eq. (1):

$$J=\frac{V}{st} \tag{1}$$

where J is the flux of the membrane (mL cm^{-2} min^{-1}), V is the volume of permeate solution (mL), and t and s are the operation time (min) and effective area of the membrane (cm^2), respectively.

Batch Mode Adsorption Experiments

A piece of membrane was added into conical flask, each of which contained 10 mL phenol methanol–water solution with different concentrations ranging from 25 mg L^{-1} to 300 mg L^{-1}. Then, it was shocked at 25°C for 12 h in a water bath oscillator. After absorption, the equilibrium concentrations of phenol in the conical flask were determined by UV spectrophotometry at a wavelength of 271 nm. The equilibrium binding amounts (q_e, mg g^{-1}) of phenol were calculated by follow equation:

$$q_e=\frac{(C_0-C_e)V}{W} \tag{2}$$

where C_0 (mg L^{-1}) and C_e (mg L^{-1}) are initial and equilibrium concentrations of phenol, respectively. V (L) and W (g) are the volume of the solution and the weight of the membrane, respectively.

Selective Recognition Experiments

To investigate the selective recognition of phenol, both SA and *p*-HB were selected as the competitive analogues. A piece of membrane (MIM or NIM) was added into a 10 mL centrifuge tube, each of which contained 10 mL the coexisting compound solution with 25 mg L^{-1} of phenol, SA, and *p*-HB, respectively. After adsorption, the binding amounts of MIM or NIM for phenol and the competitions were calculated as the procedure of static adsorption studies.

The distribution coefficient (K_d) and selectivity coefficient (α) of SA and *p*-HB with respect to phenol were obtained according to eqs. (3)–(4):[23]

$$K_d=\frac{q_e}{C_e} \tag{3}$$

K_d (mL g^{-1}) represents the distribution coefficient and q_e (mg g^{-1}) and C_e (mg L^{-1}) are the equilibrium binding amount and the equilibrium concentration of each phenol analogue in solution, respectively.

The selectivity coefficient (α) for the binding of the specific phenol analogs was obtained according to the following equation:

$$\alpha=\frac{K_{di}}{K_{di}} \tag{4}$$

where i and j represent the template and the competitive analogue, respectively.

Permeation Experiments

The permeation properties of the SAN blend membranes were evaluated through permeation tests using the mixture solutions containing 30 mg L^{-1} of phenol and SA as the feed solution. The permeation equipment used in this study contains two permeation chambers of 150 mL, resulting in an effective area of 1.5 cm^2. The membrane was fixed tightly between two chambers. The feed solution of phenol and SA (100 mL) of 30 mg L^{-1} in methanol was placed in the left-hand chamber, while

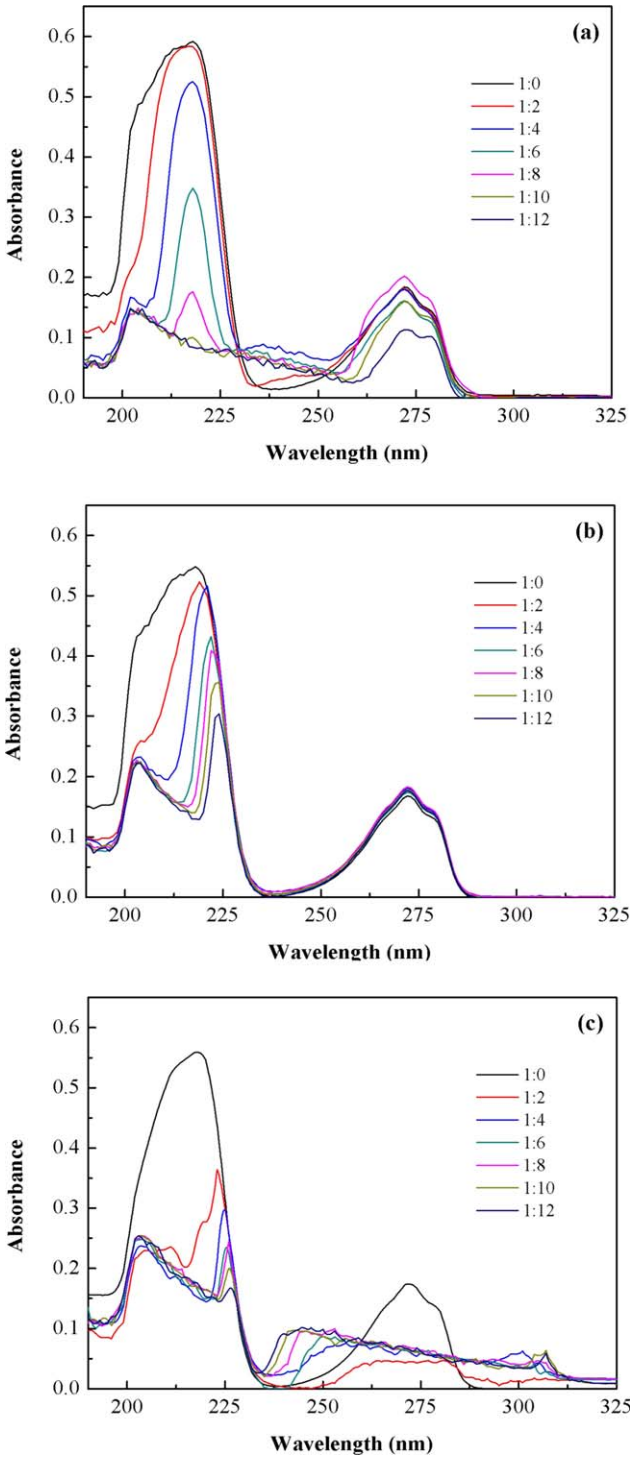

Figure 2. Adsorption spectra of the phenol (0.1 mmol L^{-1}) in the presence of various concentration (0, 0.2, 0.4, 0.6, 0.8, 1.0, 1.2 mmol L^{-1}) of three functional monomers (a: 4-VP, b: MMA, c: CA). Corresponding pure functional monomer solutions were used as blanks. [Color figure can be viewed in the online issue, which is available at wileyonlinelibrary.com.]

100 mL original methanol solution was placed in the right-hand chamber. To promote the operating accuracy, the magnetic stirrings were used to keep the solutions homogeneous at 25°C. Finally, the concentrations of both phenol and SA in the permeation mixtures were determined by a UV system at different points of sampling time.

Reusability Experiments

The reusability experiments were carried out to investigate the regeneration property of SAN blend membrane. The adsorption-desorption experiments were repeated six times by using the same imprinted membrane. During the regeneration experiment, the SAN blend imprinted membrane was tested according to the process of batch mode. Then the concentrations of phenol after adsorption were determined by a UV system and the adsorption capacity was calculated by eq. (2). Afterwards, the membrane was washed with mixed solvents of methanol/acetic acid (9 : 1, v/v) to remove the template phenol for the next adsorption–desorption cycle.

RESULTS AND DISCUSSION

UV Spectrophotometry Study

The principle of molecular imprinting lies in the formation of stable host-guest complexes prior which is obtained by binding the functional monomers and templates through hydrogen bonding, ionic bonding, or other interaction forces for polymerization.[22] Thus direct addition of template molecule to the polymeric dope solution results in formation of binding sites when the polymerization is carried out. It is of great significance in improving the interaction between the functional monomers and the templates. In the present research, 4-VP, MMA, and CA were chosen as the excellent functional monomers for host-guest type reaction, imprinting template (phenol). In order to clarify the non-covalently interactions between monomers (4-VP, MMA, and CA) and phenol, the UV-spectrometer was used for analysis and the results were shown in Figure 2.

It can be seen from Figure 2 that the maximum absorbance of phenol at 218 nm in the mixture solutions was all decreasing, which is consistent with the various concentrations of functional monomers. Moreover, the maximum adsorption wavelength showed variable shifting for each functional monomer with increasing its concentration. This is mainly due to the fact that the stable host-guest complexes were formed in the mixture through hydrogen bonding, ionic bonding or other interaction forces between the functional monomer (4-VP, MMA, and CA) and template phenol molecule. The changes of absorbance at maximum wavelength were used to judge the feasibility of the optimal molar ratio. As seen in Figure 2(a), the maximum changes of absorbance was appeared when the molar ratio of phenol to 4-VP was 1 : 6. The changes of absorbance at 218 nm were getting smaller with the increasing molar ratio of phenol to 4-VP. The result suggested that the excess amount of functional monomers might lead to increase the nonselective binding sites, which was due to the own association of molecules. Thus, after analyzing Figure 2(a–c), the optimal molar ratios of the template to functional monomers were 1 : 6, 1 : 4, and 1 : 2 for 4-VP, MMA, and CA, respectively, for the synthesis of imprinted membranes.

Transmission Electron Microscopy Measurements

The morphology and size of nano-MIPs and nano-NIPs were characterized by TEM and the results were shown in Figure 3.

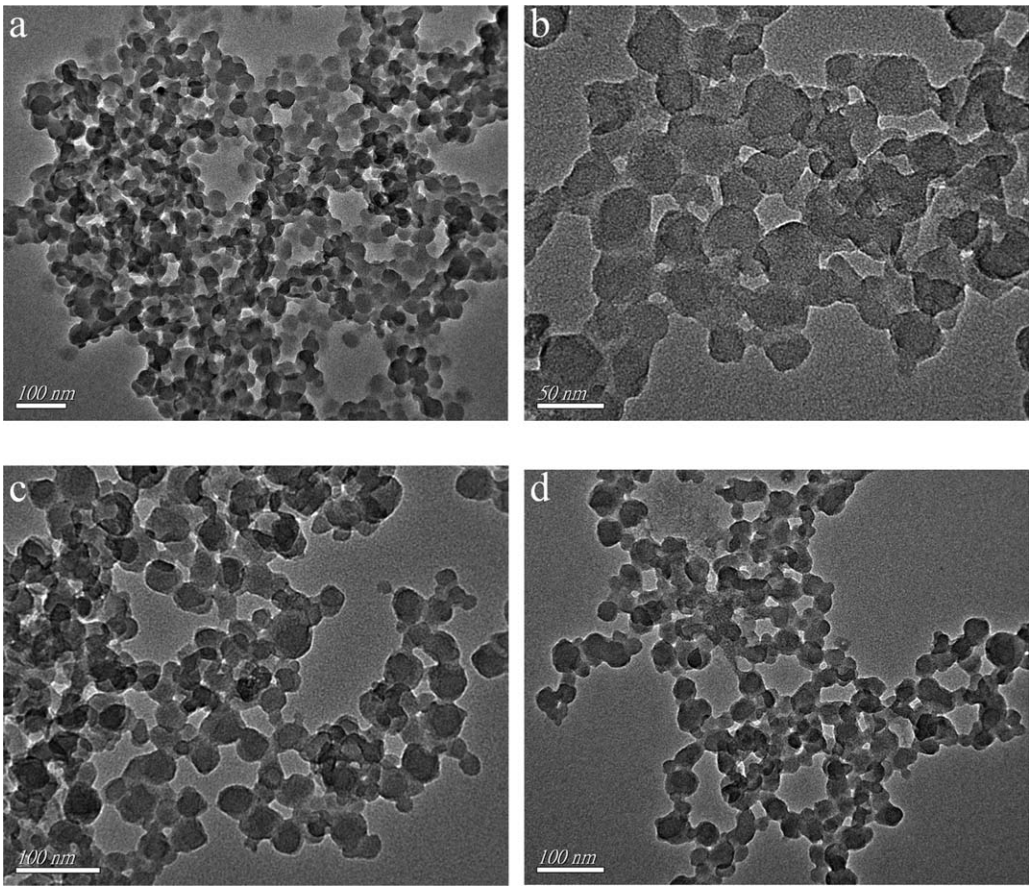

Figure 3. TEM images of (a) nano-4-VP-MIPs, (b) nano-4-VP-NIPs, (c) nano-MMA-MIPs, and (d) nano-CA-MIPs.

In Figure 3(a), TEM showed that the average diameter of nano-4-VP-MIPs was in the range of 33–38 nm by statistically analyzing the nanoparticles. In Figure 3(b), the formation of nanoparticles is observed from the morphology and size of nano-4-VP-NIPs. TEM images showed there were less difference between the morphology of nano-4-VP-MIPs and nano-4-VP-NIPs. It could be more favorable to compare the adsorption capability of membranes, including nano-4-VP-MIPs and nano-4-VP-NIPs, respectively. From Figure 3(c,d), the uniform size of nano-MMA-MIPs and nano-CA-MIPs were around 32 and 35 nm, respectively. It can be seen that the regular morphology and disperse imprinted nanoparticles were successfully synthesized by the oil-in-water emulsion polymerization process, thus to improve the selectivity of imprinted membranes.

Raman Spectroscopy

In order to ascertain the nano-MIPs with different properties, Raman spectra of nano-4-VP-MIPs, nano-MMA-MIPs, and nano-CA-MIPs were measured and showed in Figure 4. The strong bands at 1028 and 1003 cm^{-1} were correspond to the in-plane bending vibration and triangle breathing vibration of phenyl ring of polystyrene for three imprinted nanoparticles. The peak at 1595 cm^{-1}, which could be attributed to the C=N stretching vibrations of 4-VP for 4-VP-MIM1. The characteristic Raman peaks around 1728 and 1639 cm^{-1} represented the C=O and C=C stretching vibrations of MMA for nano-MMA-MIPs. The intensity of nano-CA-MIPs was increased due to the effects of phenyl ring and C=O stretching vibrations of CA. Therefore, the results revealed that the three kinds of nano-MIPs were successfully fabricated with 4-VP, MMA, and CA as functional monomers, respectively. Raman spectrum of nano-4-VP-NIPs, nano-MMA-NIPs, and nano-CA-NIPs were also

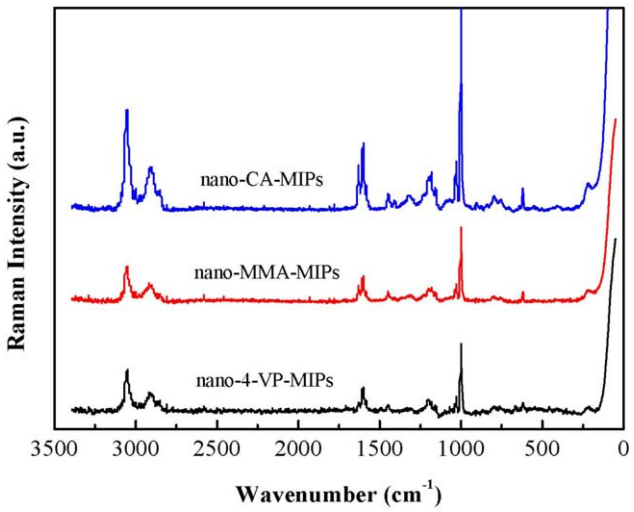

Figure 4. Raman spectrum of nano-4-VP-MIPs, nano-MMA-MIPs, and nano-CA-MIPs. [Color figure can be viewed in the online issue, which is available at wileyonlinelibrary.com.]

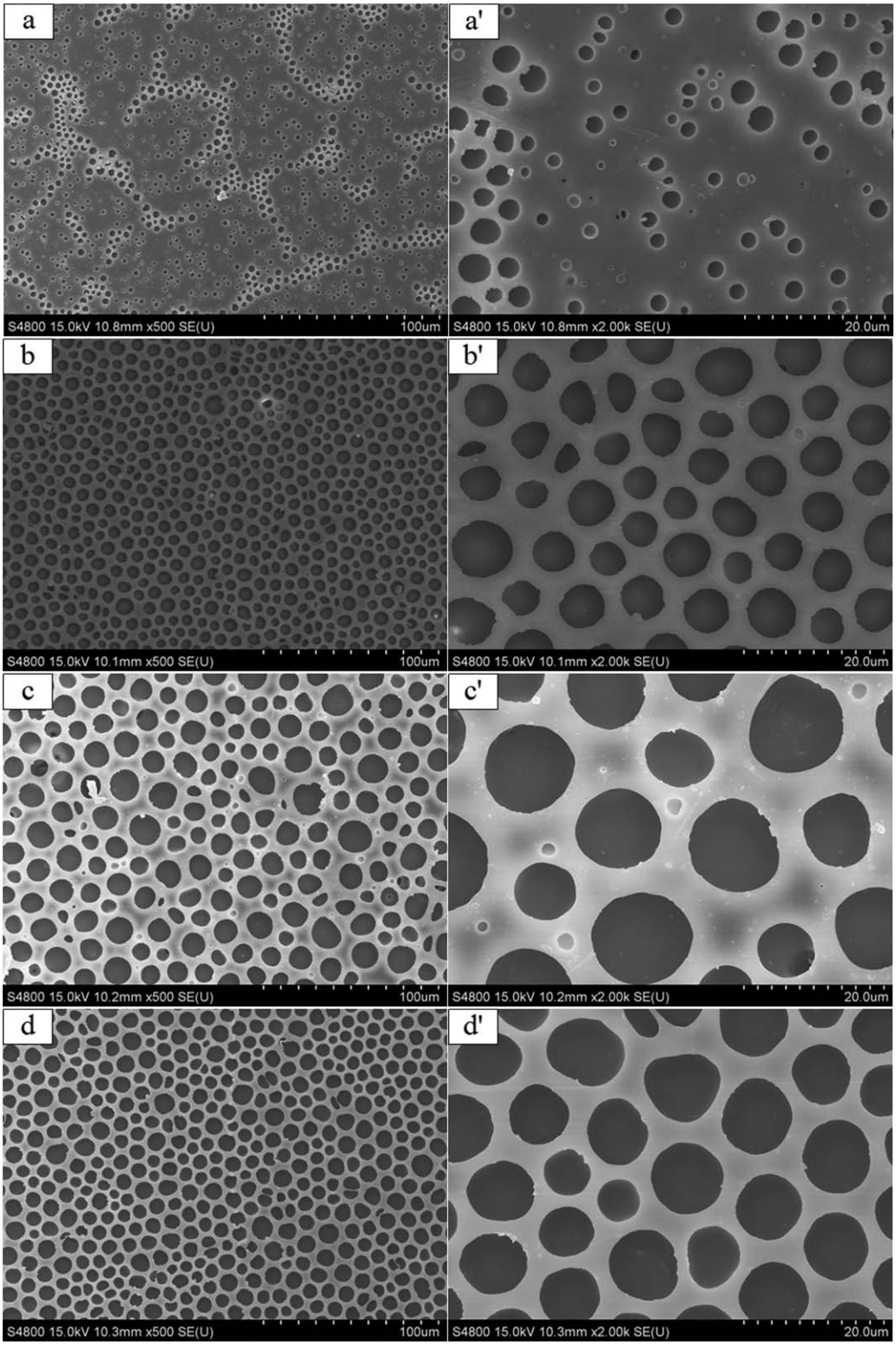

Figure 5. SEM surface micrographs of (a, a′) blank SAN membrane, (b, b′) 4-VP-MIM1, (c, c′) MMA-MIM, and (d, d′) CA-MIM.

measured (Supporting Information Figure S1). The typical peaks of Raman spectra had little difference between nano-MIPs and nano-NIPs, which could be ascribe to the similar components of nano-MIPs and nano-NIPs except for template phenol.

Scanning Electron Microscopy Analysis

The SEM images were employed to determine the effects of the nano-MIPs on the membrane morphology. As seen in Figure 5(a), blank SAN membrane showed a less porous and irregular

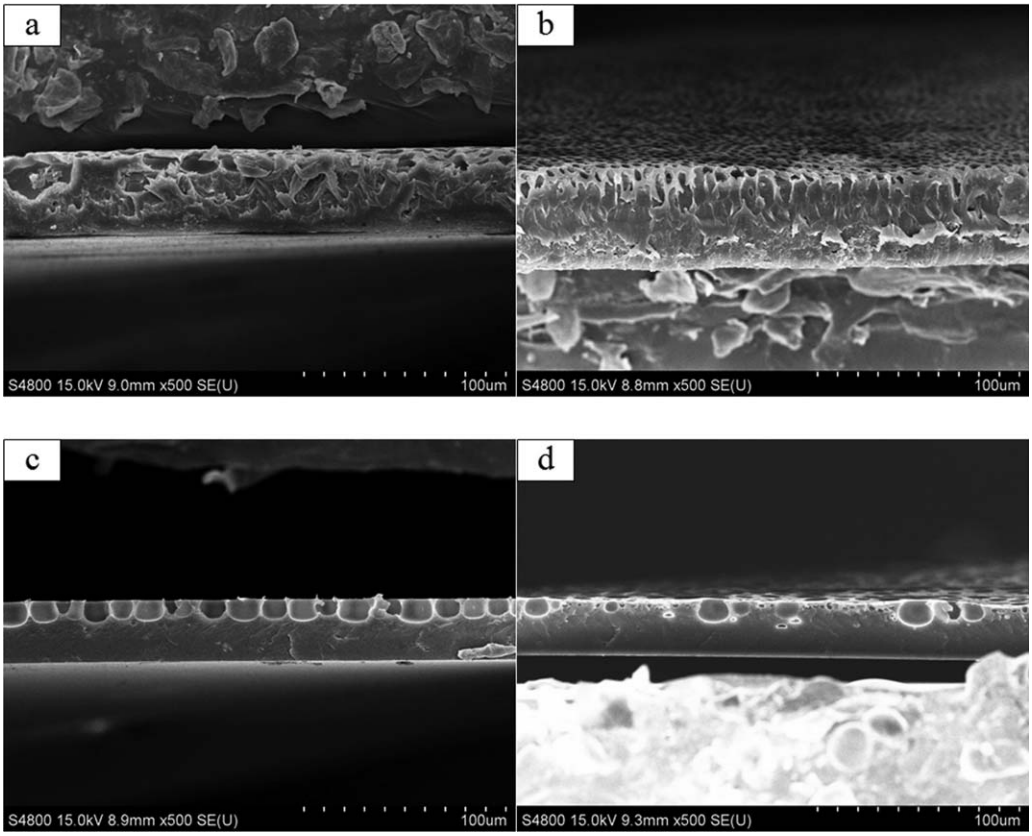

Figure 6. SEM cross-section micrographs of 4-VP-MIM (0–3) prepared at nano-4-VP-MIPs concentration of (a) 1.0 wt %, (b) 1.5 wt %, (c) 2.0 wt %, and (d) 2.5 wt %.

morphology. In Figure 5(b–d), the ordered porous surface morphologies were observed for as-prepared three imprinted membranes. Comparing with the differences in the morphology of blank SAN membrane, 4-VP-MIM1, MMA-MIM, and CA-MIM, it was found that the surface of SAN membrane was significantly changed due to the effect of nano-MIPs. The phenomena may be explained by the temperature gradient and the self-assembly of nanoparticles between aqueous phase (condensed water droplet) and oil phase (chloroform) by using BF method. When casting solution was cast onto the glass substrate to evaporate solvent, the temperature of solution surface stared to decrease. Due to the temperature gradient, water droplets were quickly condensed onto the air/casting solution interface and stabilized by casting solution layer to avoid coalescence. The nano-MIPs gathered at the interfacial between water droplets and casting solution, and played the role of segregation. The micron-sized pores were produced with the condensed water droplets as templates. As a result, the ordered porous imprinted membranes can be fabricated using the BF method in the presence of the interfacial segregation of nanoparticles. Furthermore, there were less obvious differences between 4-VP-MIM1, MMA-MIM, and CA-MIM, suggesting that the interface self-assembly of the nano-MIPs with different functional monomers for fabrications were similar, but to the imprinting effect. Consequently, combining the results of the TEM, the nano-4-VP-MIPs can be selected as the optimal imprinted nanoparticles in the present research.

The influence of nano-MIPs concentration on the final cross-sectional microstructure of the imprinted membrane was demonstrated in Figure 6. It can be seen that the porous 4-VP-MIM (0–3) were prepared in the presence of different nano-4-VP-MIPs concentrations. With increasing of the nano-4-VP-MIPs concentration, the concentration of nano-4-VP-MIPs increased in the interfacial between water droplets and casting solution, indicating that the evaporation time of water droplets became long, which was benefit for the growth of pores. However, the pore regularity of 4-VP-MIM3 is much lower than that of 4-VP-MIM2, which was ascribed to that more nano-4-VP-MIPs in casing solution prevented the water droplets from diving into the casting solution. Thereby, the pore of the 4-VP-MIM3 became irregular and smaller, as shown in Figure 6(d). Our results reveal that the ordered porous imprinted membranes can be fabricated readily using the BF method and the 4-VP-MIM2 can be chosen as the optimal imprinted membrane in this work.

Membrane Flux Experiments

The membrane flux, as one of the important membrane properties, versus operation time was determined by using transmembrane pressure of 0.15 MPa. To evaluate the effect of the imprinting technique and various functional monomers on membrane flux, the methanol solution containing 100 mg L^{-1} phenol was used as feed solution and the results were presented in Figure 7.

As shown in Figure 7(a), compared with the flux of blank SAN membrane, 4-VP-MIM1, and 4-VP-NIM1 presented higher flux values at beginning but declined later, indicating

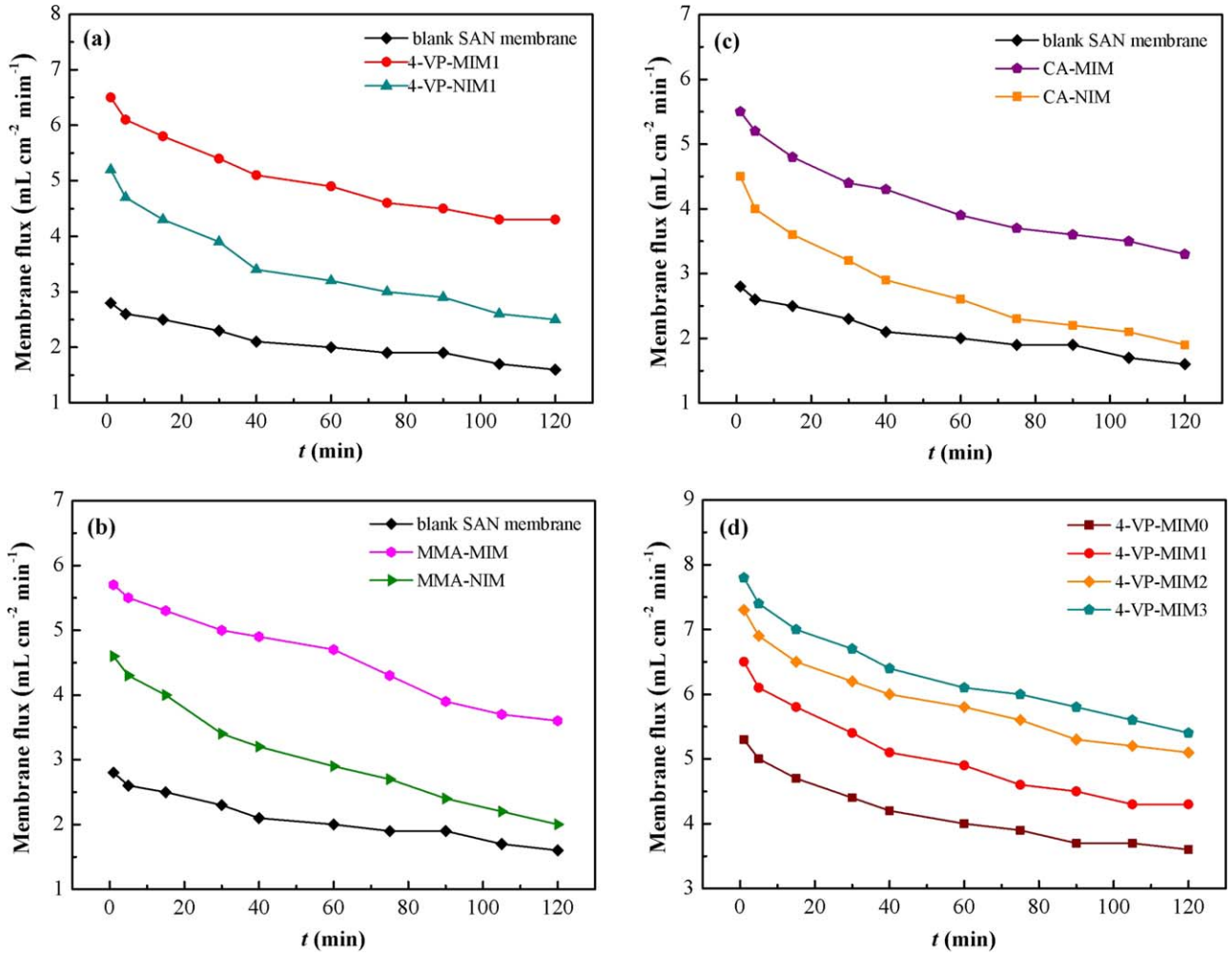

Figure 7. Membrane flux of (a) blank SAN membrane and 4-VP-MIM1/NIM1; (b) blank SAN membrane and MMA-MIM/NIM; and (c) blank SAN membrane and CA-MIM/NIM and 4-VP-MIM (0–3). [Color figure can be viewed in the online issue, which is available at wileyonlinelibrary.com.]

that the 4-VP-MIM1 and 4-VP-NIM1 had more pores and selective cavities in membrane structure than blank membranes as for the SEM results discussed in the section on scanning electron microscopy analysis. This also suggested that some of inner pores of imprinted membranes were jammed in the testing process. Thus the flux of membranes gradually declined with the increase of operation time. Moreover, the membrane flux of 4-VP-MIM1 was higher than that of 4-VP-NIM1. It is indicted that 4-VP-MIM1 with nano-4-VP-MIPs was beneficial to the accessibility of recognition sites and mass transport for phenol, which enhanced the interaction between membrane and phenol solution. Similarly, the flux profiles of MMA-MIM (or MMA-NIM) and CA-MIM (or CA-NIM) were also shown the result of high membrane flux of MIM [see Figure 7(b,c)]. However, comparing with the membrane flux values of MMA-MIM and CA-MIM, it was found that the flux of 4-VP-MIM1 was slightly higher than that of other MIMs.

Figure 7(d) presents the membrane flux profile of 4-VP-MIMs, which were prepared with various amounts of nano-4-VP-MIPs (shown in Table II). Comparing with the differences in flux values of blank SAN membrane, 4-VP-MIM0, 4-VP-MIM1, 4-VP-MIM2, and 4-VP-MIM3, it presented that the flux of SAN membrane was significantly changed after adding various amount of nano-4-VP-MIPs. With the increase of the amount of nano-4-VP-MIPs, the membrane flux of the 4-VP-MIMs seemed to be higher and the upward tendency of flux became distinct slower. It is revealed that the content of nano-MIPs facilitated the performance of membrane flux. In our study, the membrane flux of 4-VP-MIM2 was close to that of 4-VP-MIM3, which could be ascribed to that excessive nano-4-VP-MIPs in membrane limited the formation of ordered pores on membrane surface and the mass transport of phenol. Therefore, 4-VP-MIM2 is already to exhibit a decent membrane flux while precluding the phenol molecules.

Batch Adsorption Studies of Membrane

In order to investigate the adsorption capacity of phenol in the imprinted membranes with different nano-MIPs which were fabricated by polymerization in the presence of different functional monomers (4-VP, MMA, and CA) and listed in Table I, the adsorption rate and binding isotherms were carried out.

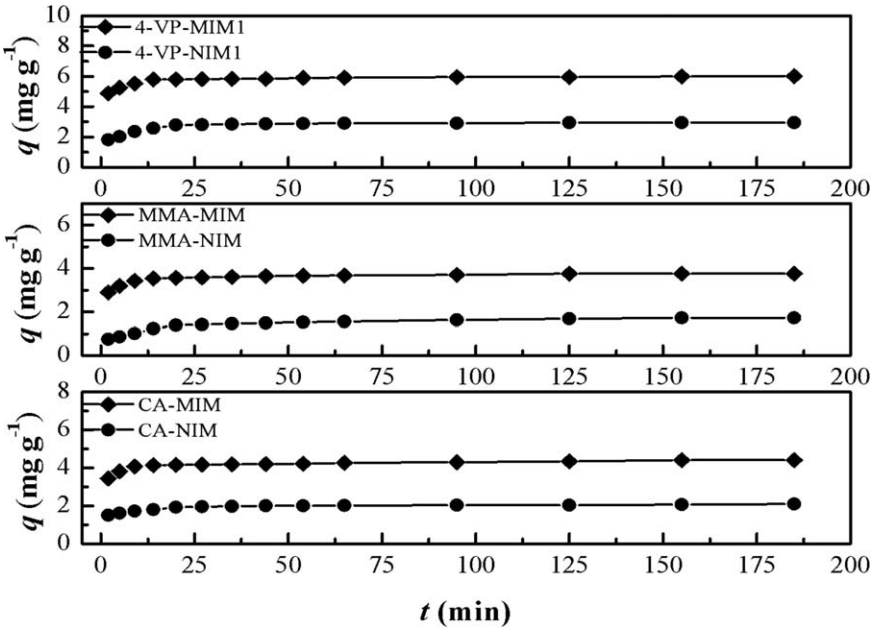

Figure 8. Comparison of the adsorption kinetics of different imprinted membranes prepared with three nano-MIPs at 25°C: (a) 4-VP-MIM1 and 4-VP-NIM1, (b) MMA-MIM and MMA-NIM, and (c) CA-MIM and CA-NIM.

The adsorption rate is a crucial parameter used to image the process of adsorption. As shown in Figure 8, the results of the adsorption capacity and equilibrium time of phenol on MIM (4-VP-MIM1, MMA-MIM, and CA-MIM) and NIM (4-VP-NIM1, MMA-NIM, and CA-NIM) were studied in this work. It can be seen that the adsorption capacities were strongly dependent on the testing time and the equilibrium time of MIM and NIM were 10 and 20 min, respectively. We speculate that the MIM reached the adsorption equilibrium faster than the NIM, which could be ascribed to more affinity imprinting cavities existed in the imprinted membranes, thus the templates were easily recognized and adsorbed by the imprinting sites. Compared with the NIM, there was a clear witness for the higher adsorption kinetics of MIM due to more and adsorption sites in the membranes. Moreover, Figure 8 presents the comparison of adsorption capacities between 4-VP-MIM1 and 4-VP-NIM1, MMA-MIM and MMA-NIM, and CA-MIM and CA-NIM, respectively. The amount of the equilibrium adsorption of

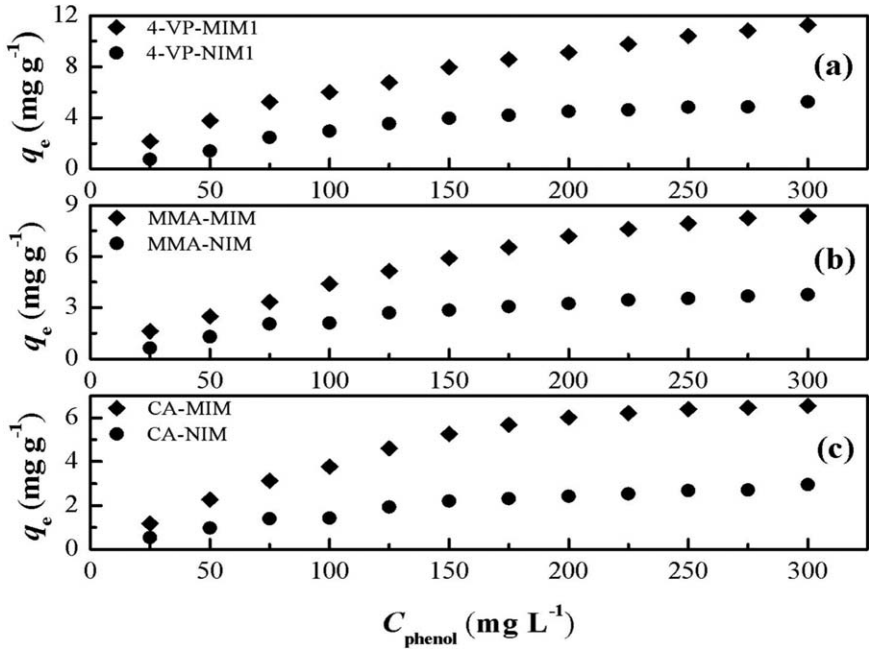

Figure 9. Comparison of the binding isotherms of different imprinted membranes prepared with three nano-MIPs at 25°C: (a) 4-VP-MIM1 and 4-VP-NIM1, (b) MMA-MIM and MMA-NIM, and (c) CA-MIM and CA-NIM.

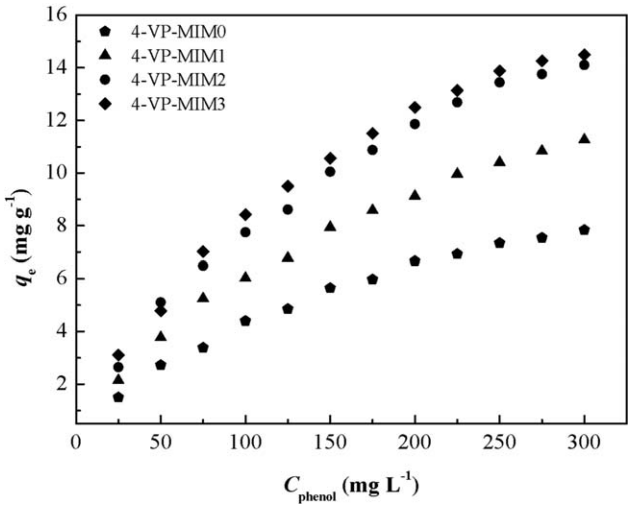

Figure 10. Adsorption isotherm curves of 4-VP-MIM0, 4-VP-MIM1, 4-VP-MIM2, and 4-VP-MIM3 at 25°C.

phenol was about 6.009 mg g^{-1} (4-VP), 3.756 mg g^{-1} (MMA), and 4.399 mg g^{-1} (CA) for MIM, and 2.951 mg g^{-1} (4-VP), 1.717 mg g^{-1} (MMA), and 2.092 mg g^{-1} (CA) for NIM, respectively. This suggested that the MIM (or NIM) synthesized with 4-VP as functional monomer adsorbed more phenol molecules than other membranes in the presence of MMA and CA. Thus, 4-VP can be selected as the effective functional monomer in this study. It is also observed that the MIM had a stronger adsorption capacity than the corresponding NIM. Therefore, the phenol molecules were much easier to access the membrane 4-VP-MIM1 containing a large number of adsorption sites.

To further study the adsorption capacity of phenol for imprinted membranes containing different functional monomers, the static equilibrium binding isotherm was investigated at 25°C for 3.0 h. Figure 9 shows the binding isotherm of various imprinted membranes for phenol at different concentration ranging from 25 to 300 mg L^{-1}. As shown in the figure, the adsorption capacities increased gradually with the increase of the concentration of phenol, whereas the MIM showed higher adsorption capacities towards phenol than NIM. As discussed before, phenol molecules were more easily accessed to MIM due to a great deal of specific binding sites in imprinted membranes, which resulting in the high adsorption capacity of MIM for phenol. It was also shown that the adsorption capacity of 4-VP-MIM1 for phenol was much stronger than that of MMA-MIM or CA-MIM. This result indicated that the MIM using 4-VP as the functional monomer was more suitable to promote the adsorption of phenol.

The amount of nano-MIPs in the imprinted membranes was expected to influence the adsorption of MIM for phenol. The phenol adsorption on the SAN membranes (4-VP-MIM0, 4-VP-MIM1, 4-VP-MIM2, and 4-VP-MIM3) prepared with various amounts of nano-4-VP-MIPs were evaluated and shown in Figure 10. With the increase of the amount of nano-4-VP-MIPs, the amount of phenol adsorption increased gradually, indicating that more imprinting sites in the imprinted membrane were beneficial for the adsorption of phenol. However, the adsorption amount of phenol for 4-VP-MIM3 was close to that on 4-VP-MIM2, which might be ascribed to that excessive nano-4-VP-MIPs in the imprinted membrane limited the recognition and adsorption capability for phenol. As discussed in SEM images, the porous surface was irregular by the effect of excessive nano-MIPs. Therefore, 4-VP-MIM2 had a better selective adsorption capability for phenol.

Selectivity Binding

In this study, the aim is to demonstrate the feasibility of the imprinted membrane that can recognize template (phenol) from mixed solution. The competitive substrates SA and *p*-HB were selected to evaluate the selective binding character of imprinted membrane. The competitive adsorption experiments were carried out by various membranes using the mixed solution containing phenol and contrast substance (SA or *p*-HB) at the concentration of 25 mg L^{-1}.

As shown in Table III, the α values of blank SAN membrane for phenol relative to SA and *p*-HB were 0.9465 and 0.9325, respectively, indicating that the blank SAN membrane was almost non-selectivity for phenol. Moreover, the α values of 4-VP-MIM1 for phenol relative to SA and *p*-HB were higher (5.0260 and 4.8660, respectively), and the corresponding α of 4-VP-NIM1 were much lower (1.8168 and 1.6768, respectively). Clearly, this presented that the MIM had stronger adsorption selectivity than that of NIM and the separation factor for SA was higher than that for *p*-HB. In addition, the experimental data showed the α values of 4-VP-MIM1, MMA-MIM, and CA-

Table III. Parameters of Batch Adsorption Selectivity of Prepared Membranes

Membrane	phenol $K_{d(phenol)}$ (L g^{-1})	α	SA $K_{d(SA)}$ (L g^{-1})
Blank SAN membrane	0.02363	0.9465	0.02497
MMA-MIM	0.08987	3.1205	0.02880
CA-MIM	0.07565	2.3115	0.03273
4-VP-MIM0	0.04495	4.2507	0.01057
4-VP-MIM1	0.09821	5.0260	0.01954
4-VP-NIM1	0.07427	1.8168	0.04088
4-VP-MIM2	0.06303	5.6770	0.01110
4-VP-MIM3	0.11535	4.8091	0.02399
Membrane	phenol $K_{d(phenol)}$ (L g^{-1})	α	*p*-HB $K_{d(p\text{-}HB)}$ (L g^{-1})
Blank SAN membrane	0.02234	0.9325	0.02396
MMA-MIM	0.08735	2.9440	0.02967
CA-MIM	0.07435	2.1515	0.03456
4-VP-MIM0	0.04254	4.0927	0.01039
4-VP-MIM1	0.09601	4.8660	0.01973
4-VP-NIM1	0.07213	1.6768	0.04302
4-VP-MIM2	0.06097	5.5433	0.01100
4-VP-MIM3	0.09535	4.6606	0.02046

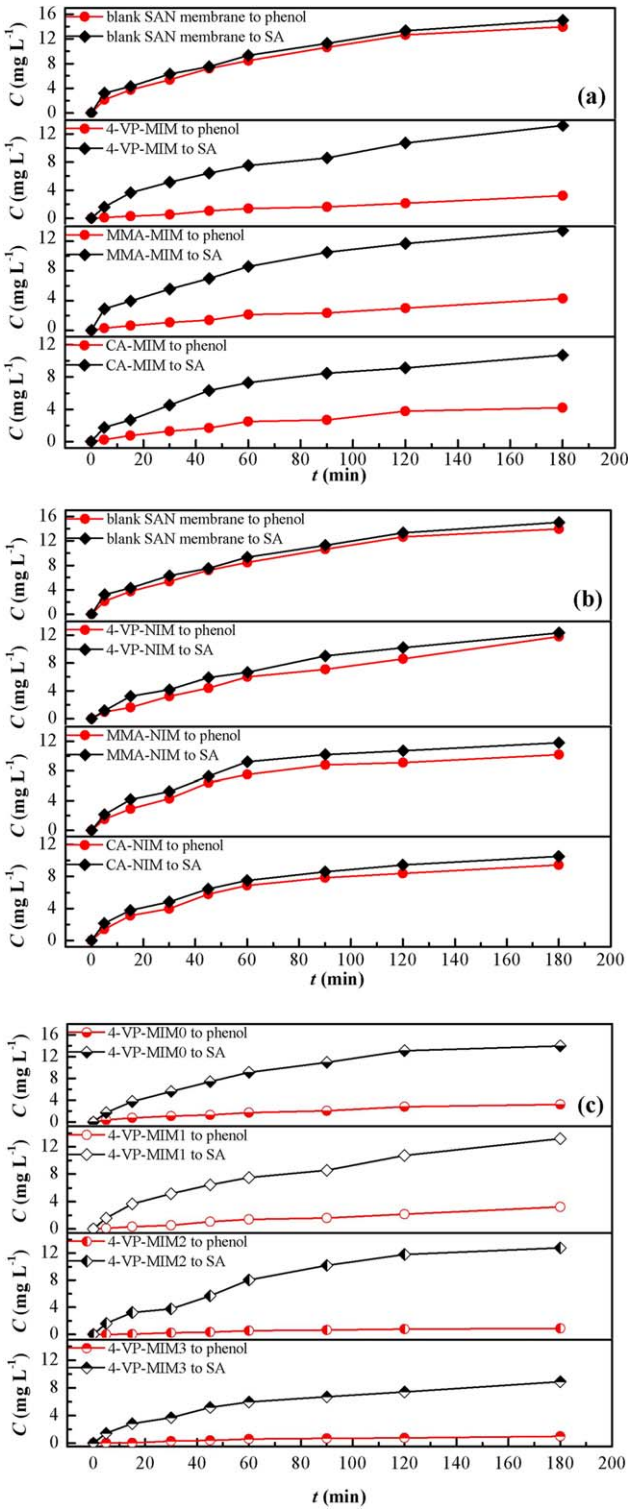

Figure 11. The time-dependent permeation curves of phenol and SA through the various membranes (feed concentration = 30 mg L^{-1}). [Color figure can be viewed in the online issue, which is available at wileyonlinelibrary.com.]

MIM for phenol in relation to SA were 5.0260, 3.1205, and 2.3115, respectively. It was obvious to find that the α value of 4-VP-MIM1 was higher than that of MMA-MIM and CA-MIM, suggesting that there were more effective adsorption sites in the 4-VP-MIM1. This revealed that the functional monomer was a crucial factor to improve the selective performance in the selective adsorption for phenol.

Furthermore, the separation effect of membrane with various amount of nano-MIPs were evaluated, thus the α values of 4-VP-MIM (0,1,2,3) for phenol in relation to SA were 4.2507, 5.0260, 5.6770, and 4.8091, respectively. Obviously, selectivity coefficient α for 4-VP-MIM3 was lower than that of 4-VP-MIM1 and 4-VP-MIM2. This indicated that the MIM with large amounts of nano-MIPs may not obtain a high performance of adsorption selectivity, which could be ascribed to the increase of nonspecific adsorption of competitive substrates. Thus the excessive nano-4-VP-MIPs in 4-VP-MIM3 may lead to limit the selective adsorption capability for phenol. Considering the above results, the 4-VP-MIM2 was the best optimizable imprinted membrane in selective adsorption for phenol.

Permeability

Figure 11 shows the perm-selectivity performance of various membranes for phenol and SA which was performed through transport-selectivity permeation tests using the permeation equipment containing two chambers. The concentration of feed mixed solution of phenol and SA through various membranes was 30 mg L^{-1}.

The time-dependent permeation curves of the blank SAN membrane and the different imprinted membranes for phenol and SA were shown in Figure 11(a). Compared to the blank SAN membrane, the concentration of phenol in the receiving chamber was much lower than that of SA for the three kinds of imprinted membranes. This result indicated that the MIMs had a special selectivity to phenol and showed the intensive binding interaction between selective recognition sites and phenol molecules during the permeation process. As expected, due to the strong interaction between imprinted membranes and templates the various imprinted membranes exhibited different levels of perm-selectivity performance for phenol. As shown in the Figure 11(a), the diffusion rate was in a descending order of phenol: blank SAN membrane, CA-MIM, MMA-MIM, and 4-VP-MIM1, which was consistent with the selective binding experiments of membranes, indicating that the 4-VP as functional monomer significantly promoted the selectivity of phenol than other functional monomers.

Figure 11(b) shows the time-dependent permeation curves of phenol and SA on the blank SAN membrane and non-printed membranes. It illustrated that the concentration of SA in the receiving chamber was close to that of phenol, while the transport rate of SA was almost equal to that of the corresponding imprinted membranes. The results illustrated that the adherence between the non-imprinted membranes and phenol (or SA) was nonspecific binding. In addition, the diffusion rate of phenol and SA for blank SAN membrane was higher than that of 4-VP-NIM1, MMA-NIM, and CA-MIM. The non-imprinted membranes with nano-NIPs owning abundant non-specific adsorption sites might limited the transport of molecules through the membranes, thus the permeation process caused slow diffusion rate of phenol and SA molecules.

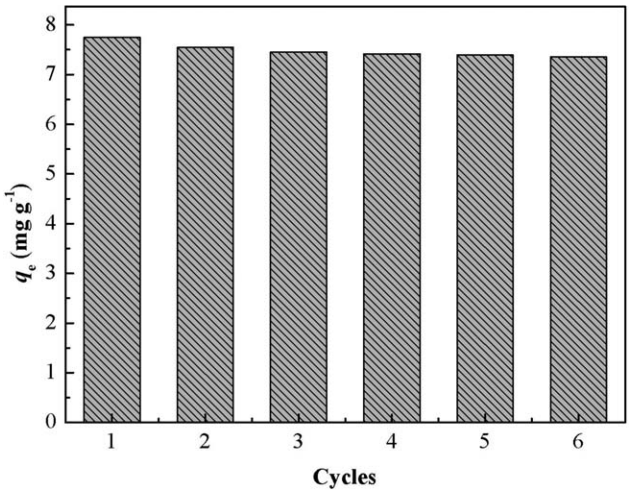

Figure 12. Reusability of the 4-VP-MIM2 at 25°C (feed concentration = 100 mg L^{-1}).

To evaluate the effect of the different content of nano-MIPs on the perm-selectivity performance, the permeation experiments of 4-VP-MIM (0,1,2,3) with different amount of nano-4-VP-MIPs were performed in this study. From Figure 11(c) we can conclude that the concentration of phenol in the test chamber measuring by a UV system was much lower than that of SA, suggesting that the 4-VP-MIM (0,1,2,3) had a high perm-selectivity for phenol. However, it presented that the concentration of phenol through 4-VP-MIM3 seemed close to that through 4-VP-MIM2, whereas the diffusion rate of SA through was lower than that through other 4-VP-MIMs. It was reasonable to assume that excessive nano-MIPs in the membranes might have a negative effect on perm-selectivity separation process due to the increasing of non-specific adsorption. Therefore, 4-VP-MIM2 had a better perm-selectivity behavior for phenol.

Reusability Experiments

In order to investigate the reusability of 4-VP-MIM2, after adsorption the imprinted membrane was regenerated using the methanol/acetic acid (9:1, v/v) mixed solvent and the deionized water. The adsorption–desorption experiment was repeated six times using the same imprinted membrane, and then the adsorption capacity was presented in Figure 12. It was found that the 4-VP-MIM2 could be effectively reused for six times with only about 4.65% loss of initial adsorption capacity. It can be concluded that the 4-VP-MIM2 can be reused at least six times with their high adsorption capacity.

CONCLUSION

In the present work, a series of ordered microporous SAN blend imprinted membranes for template phenol were successfully synthesized by BF method. It made the imprinted nanoparticles (nano-MIPs) dispersed in organic solvents including a large number of imprinting sites. Results from membrane flux suggested that the regular patterned membranes with nano-MIPs led to high and stable membrane flux profiles but the blank SAN membrane had the lowest membrane flux. Moreover, the as-formed ordered porous morphology improved the imprinting performance of nano-MIPs in membranes. The adsorption performance, selective binding ability and permeation selectivity of the MIM depended on the functional monomers and the amount of nano-MIPs in the membranes. The 4-VP-MIM2 was found to be the optimal imprinted membrane to increase the separation effect and adsorption capacity on phenol. The selectivity adsorption experiments revealed that the 4-VP-MIM2 had excellent selective recognition ability for the phenol relative to SA. In addition, adsorption analysis suggested that the 4-VP-MIM2 showed high ability to separate the template phenol from aqueous solution. The permselectivity performance of 4-VP-MIM2 was also greatly enhanced due to the addition of appropriate 4-VP imprinted nanoparticles (nano-4-VP-MIPs). Furthermore, this work has opened a novel and effective way to separate and concentrate phenol from SA, which is useful in purification of SA in the complex matrix.

NOMENCLATURE

MIP	molecularly imprinted polymer
NIP	molecularly non-imprinted polymer
MIT	molecularly imprinting technology
MIM	molecularly imprinted membrane
NIM	molecularly non-imprinted membrane
BF	breath figure
SAN	styrene-acrylonitrile copolymer
4-VP	4-vinyl pyridine
MMA	methyl methacrylate
CA	cinnamic acid
SA	salicylic acid
p-HB	*p*-hydroxybenzoic
ASA	acetylsalicylic acid
PVDF	poly(vinylidene fluoride)
Ars	artemisinin
PVC	polyvinyl chloride
St	styrene
DTAB	dodecyltrimethylammonium bromide
KPS	potassium persulfate
DVB	divinylbenzene
RH	relative humidity
J	flux (L m^{-2} h^{-1})
t	sampling time (h)
s	effective area (m^2)
q	binding amount (mg g^{-1})
K_d	distribution coefficients

Greek letters

α	selectivity coefficients

ACKNOWLEDGMENTS

This work was financially supported by the National Natural Science Foundation of China (Nos. 21207051, 21406085), Ph.D. Programs Foundation of Ministry of Education of China (No. 20123227120015) and Natural Science Foundation of Jiangsu Province (BK20140580), and Special Financial Grant from the China Postdoctoral Science Foundation (2014T70488).

REFERENCES

1. Jafari, M. T.; Badihi, Z.; Jazan, E. *Talanta* **2012**, *99*, 520.

2. Meng, M. J.; Feng, Y. H.; Zhang, M.; Ji, Y. J.; Dai, J. D.; Liu, Y.; Yu, P.; Yan, Y. S. *Chem. Eng. J.* **2013**, *231*, 132.
3. Huang, J. X.; Hu, Y. F.; Hu, Y. L.; Li, G. K. *Talanta* **2013**, *107*, 49.
4. Alshehri, S. M.; Naushad, M.; Ahamad, T.; Alothman, Z. A.; Aldalbahi, A. *Chem. Eng. J.* **2014**, *254*, 181.
5. Wulff, G.; Sarhan, A. *Angew. Chem. Int. Ed. Engl.* **1972**, *11*, 341.
6. Wang, J. Y.; Xu, Z. L.; Wu, P.; Yin, S. J. *J. Membr. Sci.* **2009**, *331*, 84.
7. Blanco, S. G. D.; Donato, L.; Drioli, E. *Sep. Purif. Technol.* **2012**, *87*, 40.
8. Alizadeh, T. *Anal. Chim. Act.* **2008**, *623*, 101.
9. Zhang, Y. Q.; Shan, X.; Gao, X. Q. *Sep. Purif. Technol.* **2011**, *76*, 337.
10. Wu, Y. L.; Meng, M. J.; Liu, X. L.; Li, C. X.; Zhang, M.; Ji, Y. J.; Sun, F. Q.; He, Z. H.; Yan, Y. S. *Sep. Purif. Technol.* **2014**, *131*, 117.
11. Donato, L.; Tasselli, F.; De Luca, G.; Garcia Del Blanco, S.; Drioli, E. *Sep. Purif. Technol.* **2013**, *116*, 184.
12. Dima, S. O.; Meouche, W.; Dobre, T.; Nicolescu, T. V.; Sarbu, A. *React. Funct. Polym.* **2013**, *73*, 1188.
13. Li, X. F.; Wang, Y.; Zhang, L.; Tan, S. X.; Yu, X. L.; Zhao, N.; Chen, G. Q.; Xu, J. *J. Colloid Interface Sci.* **2010**, *350*, 253.
14. Bormashenko, E.; Balter, S.; Bormashenko, Y.; Aurbach, D. *Colloids Surf. Physicochem. Eng. Aspect.* **2012**, *415*, 394.
15. Widawski, G.; Rawiso, M.; François, B. *Nature* **1994**, *369*, 387.
16. Escalé, P.; Rubatat, L.; Billon, L.; Save, M. *Eur. Polym. J.* **2012**, *48*, 1001.
17. Liu, C. X.; Lang, W. Z.; Shi, B. B.; Guo, Y. *J. Mater. Lett.* **2013**, *107*, 53.
18. Han, Y. Q.; Zhang, Q.; Han, F. L.; Li, C. X.; Sun, J. F.; Lu, Y. *Polymer* **2012**, *53*, 2599.
19. Tu, Z. K.; Tang, H. L.; Shen, X. T. *ACS Appl. Mater. Interfaces.* **2014**, *6*, 12931.
20. Margulis-Goshen, K.; Magdassi, S. *Curr. Opin. Colloid Interface Sci.* **2012**, *17*, 290.
21. Chang, C. C.; Juang, T. Y.; Ting, W. H.; Lin, M. S.; Yeh, C. M.; Dai, S. H. A.; Suen, S. Y.; Liu, Y. L.; Jeng, R. J. *Mater. Chem. Phys.* **2011**, *128*, 157.
22. Ma, H. Y.; Tian, Y.; Wang, X. L. *Polymer* **2011**, *52*, 489.
23. Meng, M. J.; Wang, Z. P.; Ma, L. L.; Zhang, M.; Wang, J.; Dai, X. H.; Yan, Y. S. *Ind. Eng. Chem. Res.* **2012**, *51*, 14915.